Effects of Unbalanced Mains Voltage Conditions on Three-Phase Hybrid Rectifiers Employing Third Harmonic Injection

M. Makoschitz*, M. Hartmann†, and H. Ertl*
* Institute of Energy Systems and Electrical Drives, Power Electronics Section
University of Technology Vienna, Austria; Email: markus.makoschitz@tuwien.ac.at

† Schneider Electric Power Drives, Section Drives, Power Conversion
Vienna, Austria; Email: michael.hartmann@ieee.org

***Abstract*—Multitudinous industry applications require single-phase or three-phase rectification circuits. Hybrid rectifiers offer fairly flexible fields of applications (compared to purely implemented passive or active rectifiers) due to their optional active converter topology. The low harmonic input stage, however, is in general exposed to unbalanced AC-side mains voltage conditions. Depending on location and/or facility, input voltage variations can be 3% or higher (short-term). Imbalance in mains input voltages on hybrid rectifiers which are employing the third harmonic injection principle are therefore analysed in detail. It is shown that unbalanced AC-side input voltages not only directly influence THD of input currents and power factor of the system, but also increase current stress of active switches and passive components. Basic considerations are discussed from a mathematical point of view and are finally confirmed by simulation and experimental results of a 10 kW/10 kHz laboratory prototype (passive three-phase diode bridge rectifier equipped with 'Flying' Converter Cell (FCC) active current injection cell).**

***Index Terms*—Three-Phase AC-DC Conversion, Unbalanced Mains Voltage Condition, Unbalanced Grid Voltage, Input Current Quality, Third-Harmonic Injection**

I. Introduction

Passive, hybrid and active rectifier circuits play a major role in todays electric systems. Whenever a device needs to be feed by DC voltage input which has to be formed by AC input voltages, one of these rectification circuits form the interconnection between AC- and DC-side. Hybrid [1]–[3] and active [4] rectifiers offer unity power factor λ, low harmonic input current distortions $\mathrm{THD_i}$.

In general rectifier circuits have to operate under unbalanced grid voltage conditions (grid voltage sag conditions, voltage surges,...). Imbalance in grid voltages – typically caused due to unbalanced loads or renewable energy systems (wind power applications, photovoltaic systems,...) in weak power system networks – may result in deterioriaton of the rectifiers input and output characteristics. In addition, not only mains voltages, but also line impedances must be considered as unbalanced.

In order to deal with side-effects of unbalanced grid voltages as e.g. negative sequence voltage, advanced control strategies are required to guarantee input current quality and supress even harmonics on the DC-side of the system. Regarding rectifier systems as for example the VIENNA rectifier [5]–[8], the six switch rectifier [9]–[14], the active shunt power filter [15], [16] or the indirect matrix converter (IMC) [17] numerous control methods are proposed (given references). One promising control strategy (for e.g. the six switch rectifier) is the improved direct power control which not only utilizes the active power but also the appearing reactive power due to imbalance in grid voltages for control. Other control strategies as voltage oriented control (VOC) or model predictive direct power control (MPDPC) for PWM rectifiers are similarly leading to promising results.

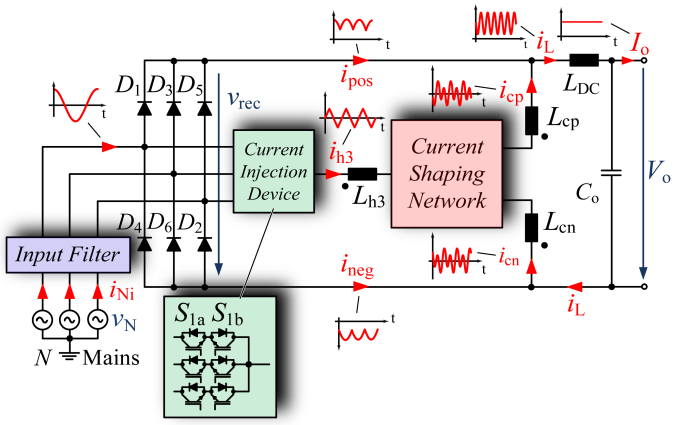

Fig. 1: Basic schematic of passive three-phase rectifier employing an active current shaping and injection network in order to achieve sinusoidal mains currents i_{Ni}.

Considering hybrid rectifiers with optionally active circuit based on the third harmonic injection principle (illustrated in **Fig. 1** and discussed in [18]), it is not quite clear up to now, in which way heavily unbalanced mains voltage conditions may affect the injection circuit. A concise mathematical evaluation on the effects of abnormal mains voltage conditions on these rectifier circuits is therefore given in this paper. The next section is hence briefly engaged in comparing common mathematical instruments which appear to be suitable for upcoming investigations. A set of basic equations is therefore provided for further advanced mathematical analysis. Basic calculations are finally confirmed by simulation and experimental results of a 10 kW/10 kHz laboratory prototype utilizing a FCC as discussed in [19]–[21].

II. Mathematical Investigation Strategies

This section briefly discusses and compares 3 different mathematical approaches (mathematical investigation applying "fouriercoefficient-theory", "sector-by-sector description" and "approximation of the DC-side smoothing inductance current i_L") which may be applicable for further analyses and postulates a set of basic equations which are useful for further calculations considering perfectly balanced mains voltage conditions.

A. Fouriercoefficients

In general, fourier series (applying fourier coefficients) can be used to describe a periodic signal utilizing the sum of sets of sinusodial functions (valid for all values of φ_N ($\varphi_\mathrm{N} \in [-\infty \dots \infty]$)). According to fourier-theory, coefficients c_k can be calculated using

$$c_k = \frac{1}{2\pi} \int_0^{2\pi} f(\varphi_\mathrm{N})\, e^{-jk\varphi_\mathrm{N}}\, \mathrm{d}\varphi_\mathrm{N} \tag{1}$$

whereby k denotes the multiple of the fundamental frequency. The analog signal which can be now expressed by fundamental frequency and higher order components can be finally recomposed by

$$f(\varphi_\mathrm{N}) = c_0 + \sum_{k=1}^{\infty} \frac{|c_k|}{2} \sin(k\varphi_\mathrm{N}) \ . \tag{2}$$

Applying these equations for obtaining output voltages of the positive and negative busbar of the passive rectifier (v_pos and v_neg) and the third harmonic voltage v_h3, the respective signals calculate to

$$\begin{aligned} v_\mathrm{pos} &= \frac{3\sqrt{3}\hat{V}_\mathrm{N}}{\pi} \left(\frac{1}{2} + \sum_{k=1,2,3,\dots}^{\infty} \frac{(-1)^{k+1}}{(3k)^2 - 1} \cos(3k\varphi_\mathrm{N}) \right) \\ v_\mathrm{neg} &= \frac{3\sqrt{3}\hat{V}_\mathrm{N}}{\pi} \left(-\frac{1}{2} + \sum_{k=1,2,3,\dots}^{\infty} \frac{1}{(3k)^2 - 1} \cos(3k\varphi_\mathrm{N}) \right) \\ v_\mathrm{h3} &= -\frac{3\sqrt{3}\hat{V}_\mathrm{N}}{\pi} \left(\sum_{k=1,3,5,\dots}^{\infty} \frac{2}{(3k)^2 - 1} \cos(3k\varphi_\mathrm{N}) \right) \ . \end{aligned} \tag{3}$$

The rectifier output voltage v_rec can now easily be calculated by $v_\mathrm{pos} - v_\mathrm{neg}$ and hence yields

$$v_\mathrm{rec} = \frac{3\sqrt{3}\hat{V}_\mathrm{N}}{\pi} \left(1 - \sum_{k=1,2,3,\dots}^{\infty} \frac{2}{(6k)^2 - 1} \cos(6k\varphi_\mathrm{N}) \right) \ . \tag{4}$$

Taking a closer look at the assessed equations it can be seen that the voltages v_pos, v_neg and v_h3 show a dominant third order harmonic whereas v_rec is defined by multiples of sixth order spectral components. It can therefore be assumed that i_L is also showing this dominant sixth order harmonic which has to be compensated by the current injection network.

The mean value of the output voltage V_o of the system for balanced input voltages can be recorded as

$$V_\mathrm{o} = 3\sqrt{3}\hat{V}_\mathrm{N}/\pi \ . \tag{5}$$

These equations allow to form the DC-side smoothing inductance voltage $v_{L_\mathrm{DC}} = v_\mathrm{rec} - V_\mathrm{o}$ and the output filter current i_L can hence be calculated by using

$$i_\mathrm{L}(\varphi_\mathrm{N}) = \frac{1}{\omega_\mathrm{N} L_\mathrm{DC}} \int v_{L_\mathrm{DC}}(\varphi_\mathrm{N})\, \mathrm{d}\varphi_\mathrm{N} \tag{6}$$

which finally leads to

$$i_\mathrm{L}(\varphi_\mathrm{N}) = I_\mathrm{o} - \frac{3\sqrt{3}\hat{V}_\mathrm{N}}{\pi\omega_\mathrm{N} L_\mathrm{DC}} \sum_{k}^{\infty} \frac{2}{(6k)^3 - 6k} \sin(6k\varphi_\mathrm{N}). \tag{7}$$

Thus, the output voltage ripple of C_o which is defined by

$$v_\mathrm{o,ac}(\varphi_\mathrm{N}) = \frac{1}{\omega_\mathrm{N} C_\mathrm{o}} \int (i_\mathrm{L} - I_\mathrm{o})(\varphi_\mathrm{N})\, \mathrm{d}\varphi_\mathrm{N}. \tag{8}$$

is primarily characterised by the current ripple of the DC-side choke of the three-phase hybrid rectifier system and computes to

$$v_\mathrm{o,ac}(\varphi_\mathrm{N}) = \frac{3\sqrt{3}\hat{V}_\mathrm{N}}{\pi\omega_\mathrm{N}^2 L_\mathrm{DC} C_\mathrm{o}} \sum_{k}^{\infty} \frac{2}{(6k)^4 - (6k)^2} \cos(6k\varphi_\mathrm{N}). \tag{9}$$

If only passive rectification of the system is considered (injection circuit deactivated) the input currents i_Ni are constituted by shapes of i_L. Evaluating the converging values of the appropriate sum-function after integrating the squared value of i_Ni, the input RMS currents values can be finally determined – after putting in some calculation effort – to

$$B_6\text{-}I_\mathrm{Ni,rms} = \sqrt{\frac{2}{3} I_\mathrm{o}^2 + \left(\frac{7}{6}\pi^2 + \frac{9\sqrt{3}}{2}\pi - 36 \right) \left(\frac{\hat{V}_\mathrm{N}}{\pi\omega_\mathrm{N} L_\mathrm{DC}} \right)^2} \tag{10}$$

B. Sector by Sector Description

One of the easiest ways to describe voltage and current waveforms of a three-phase rectifier is "sector by sector" evaluation. As the name indicates, voltage and current waveforms are calculated by merely considering a specific sector (e.g. $\varphi_\mathrm{N} \in \left[0 \dots \frac{\pi}{3}\right]$) which is typically specified due to the signal waveforms. The major advantage of this method is that the mathematical description typically shows a very low grade of complexity for a simplified (neglecting parasitic components etc.) model of the rectifier. As all signals show an (at least) 2π-periodicity, not much calculation effort has therefore be taken into account. Voltage signals of the rectifier (v_pos, v_neg and v_h3) for the sector $\varphi_\mathrm{N} \in \left[0 \dots \frac{\pi}{3}\right]$ are hence given by

$$\begin{aligned} v_\mathrm{pos} &= \hat{V}_\mathrm{N} \cos(\varphi_\mathrm{N}) \\ v_\mathrm{h3} &= \hat{V}_\mathrm{N} \cos\left(\varphi_\mathrm{N} - \frac{2\pi}{3}\right) \\ v_\mathrm{neg} &= \hat{V}_\mathrm{N} \cos\left(\varphi_\mathrm{N} - \frac{4\pi}{3}\right) \ . \end{aligned} \tag{11}$$

The instantaneous diode bridge output voltage can hence be described by

$$v_\mathrm{rec} = -\sqrt{3}\hat{V}_\mathrm{N} \sin\left(\varphi_\mathrm{N} - \frac{2\pi}{3}\right) \tag{12}$$

TABLE I: Comparison of analytical analysis of passive three-phase rectifier systems using different mathematical tools including "fourier series" (FS), "sector by sector evaluation" (SbS) or simple "approximation of i_L" (Approx). I_rms, $I_\mathrm{fund,rms}$ and the $\mathrm{THD_i}$ are evaluated at $V_\mathrm{N,rms} = 230\,\mathrm{V}$, $f_\mathrm{N} = 50\,\mathrm{Hz}$, $P_\mathrm{o} = 10\,\mathrm{kW}$, $L_\mathrm{DC} = 2.25\,\mathrm{mH}$. L_DC is calculated for $V_\mathrm{N,rms} = 230\,\mathrm{V}$, $f_\mathrm{N} = 50\,\mathrm{Hz}$, $P_\mathrm{o} = 10\,\mathrm{kW}$, $\mathrm{THD_i} = 40\,\%$

Comparison of Results			
	FS	SbS	Approx
B_6-I_rms [A]	15.752	15.752	15.737
B_6-$I_\mathrm{fund,rms}$ [A]	14.530	14.530	14.525
B_6-$\mathrm{THD_i}$ [%]	41.943	41.943	41.696
L_DC [mH]	2.507	2.507	2.485

and the mean output voltage of the system for one mains period (2π) can be assessed by

$$V_\mathrm{o} = \frac{3\sqrt{3}\hat{V}_\mathrm{N}}{\pi} \tag{13}$$

which perfectly equals the determined output voltage V_o as derived in the previous subsection II.A. The DC-side injection current i_L computes to

$$i_\mathrm{L} = I_\mathrm{o} + \frac{3\sqrt{3}\hat{V}_\mathrm{N}}{\omega_\mathrm{N} L_\mathrm{DC}} \left(\frac{1}{6} + \frac{1}{3}\cos\left(\varphi_\mathrm{N} - \frac{2\pi}{3}\right) - \frac{1}{\pi}\varphi_\mathrm{N} \right) \tag{14}$$

and finally the resulting instantaneous output voltage ripple therefore computes to

$$\begin{aligned} v_\mathrm{o,ac} = \frac{3\sqrt{3}\hat{V}_\mathrm{N}}{2\omega_\mathrm{N}^2 L_\mathrm{DC} C_\mathrm{o}} \Bigg(& \varphi_\mathrm{N}^2 + \frac{1}{3}\varphi_\mathrm{N} + \dots \\ & \dots + \frac{2}{3}\sin\left(\varphi_\mathrm{N} - \frac{2\pi}{3}\right) - \left(\alpha_\mathrm{C}^2 + \frac{1}{3}\alpha_\mathrm{C} + \frac{2}{\pi}\right) \Bigg) . \end{aligned} \tag{15}$$

α_C denotes the angle where $V_\mathrm{o} = v_\mathrm{rec}$, and therefore, $v_\mathrm{o}(\varphi_\mathrm{N}) = V_\mathrm{o}$. The maximum of i_L is also located at this specific time instant. It has to be noted that α_C can be evaluated with

$$\alpha_\mathrm{C} = -\frac{\pi}{3} + \arcsin\left(\frac{3}{\pi}\right) . \tag{16}$$

Similar to the "fourier-coefficient" approach, the input currents i_Ni are assembled by shapes of i_L (merely passive rectification considered). Finding the squared root of integrated squared shapes of i_L over one mains period (2π) leads to an input current RMS value of

$$B_6\text{-}I_\mathrm{Ni,rms} = \sqrt{\frac{2}{3}I_\mathrm{o}^2 + \left(\frac{7}{6}\pi^2 + \frac{9\sqrt{3}}{2}\pi - 36\right)\left(\frac{\hat{V}_\mathrm{N}}{\pi\omega_\mathrm{N} L_\mathrm{DC}}\right)^2} \tag{17}$$

C. Approximation of i_L

The last approach for analysing the hybrid rectifier tries to take affort of both previously mentioned mathematical tools. On the one hand, the typical section by section analysis may be applied. On the other hand, the DC-side smoothing inductor current i_L may be rewritten as an approximation of the fourier series results, however, preventing the notation of a sum-function. As proposed in [19] and obviously taking advantage of previously made assumptions, the approximated DC-side smoothing inductance current i_L can be written as

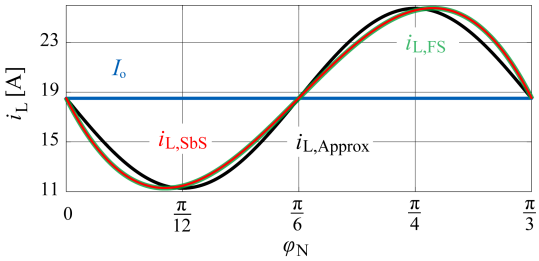

Fig. 2: Different calculation efforts for the DC-side smoothing inductor current i_L considering "sector by sector" ($i_\mathrm{L,SbS}$), "fourier series" ($i_\mathrm{L,FS}$) and "current approximation" ($i_\mathrm{L,Approx}$) for 10kW output power (P_o)

$$i_\mathrm{L} = I_\mathrm{o} + \hat{I}_\mathrm{L,ac}\sin(6\varphi_N) \tag{18}$$

by neglecting higher order harmonics. The peak value of the current ripple can thereofre easly be computed via

$$\hat{I}_\mathrm{L,ac} = \frac{1}{\omega_\mathrm{N} L_\mathrm{DC}} \int_{-\arccos\left(\frac{3}{\pi}\right)}^{\arccos\left(\frac{3}{\pi}\right)} \left(v_\mathrm{rec}(\varphi_\mathrm{N}) - V_\mathrm{o}\right)(\varphi_\mathrm{N})\,\mathrm{d}\varphi_\mathrm{N} \tag{19}$$

which finally leads to

$$\hat{I}_\mathrm{L,ac} = \frac{3\sqrt{3}\hat{V}_\mathrm{N}}{\pi\omega_N L_\mathrm{DC}} \left[\sqrt{\left(\frac{\pi}{3}\right)^2 - 1} - \arccos\left(\frac{3}{\pi}\right) \right] . \tag{20}$$

The RMS values of the passive systems AC-side mains currents result in

$$B_6\text{-}I_\mathrm{Ni,rms} = \sqrt{\frac{2}{3}I_\mathrm{o}^2 + \frac{1}{3}\hat{I}_\mathrm{L,ac}^2} \tag{21}$$

D. Comparison of Results

In order to compare all previously discussed results, the analytically derived formulas for input currents RMS, input currents fundamental RMS[1], DC side smoothing inductance[1] and total harmonic distortion[1] of the AC-side input currents have been evaluated numerically.

As can be seen from TABLE I there is no loss of accuracy while choosing "fourier series" or "sector by sector" signal evaluation. However, a diminutive deviation considering the approximation of i_L compared to "sector by sector" analysis can be observed. The relative error for input current RMS and fundamental RMS value amounts to 0.1 % and 0.04 %, respectively. For $\mathrm{THD_i}$ and L_DC a relative error of 0.59 % and 0.87 % can be noticed, respectively. To sum up, the achieved results of all three applied mathematical instruments are totally valid and merely varying in complexity. Depending on accuracy, there is not much difference for numerically evaluated values. Only the current waveform of the approximated DC-side smoothing inductance current i_L slighty differs, compared to evaluted currents regarding "sector by sector" or "fourier series" computation (cf. **Fig. 2**). It can be observered that

[1]not discribed in this work analytically

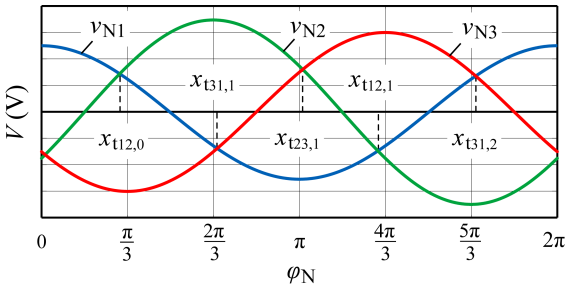

Fig. 3: Unsymmetrical mains voltages v_{N1}-v_{N3} applying $V_{N1,rms} \neq V_{N2,rms} \neq V_{N3,rms}$. Calculated new time instants $x_{tij,k}$ are deviating from the typically assumed instants $\frac{2\cdot(k-1)\pi}{3}$ considering balanced mains voltage condition.

"fourier series" and " sector by sector" calculation are perfectly aligned from a graphical point of view. "Current approximation" shows a purely sinusoidal signal characteristic and is hence missing its higher harmonics. It is therefore slightly diverging compared to the exact evaluated waveforms. It should be noted that all mathematical approaches for analyzing the inductor current show the same "zero crossings" considering $i_L - I_o$ for a specific sector $\left(\varphi_N \in \left[0 \dots \frac{\pi}{3}\right]\right)$.

III. Effects of Unbalanced Mains Voltages

Section II listed some basic equations for a hybrid rectifier employing third harmonic injection, including a three-phase passive diode bridge rectifier considering well-balanced mains voltages $V_{N1,rms} = V_{N2,rms} = V_{N3,rms}$. According to the EN 50160 standard, it is stated that supply voltage variations should not exceed $\pm 10\,\%$ of the nominal voltage $V_{N,rms}$ (periods with interruptions excluded).
In the following, the impact of unbalanced mains voltages on hybrid three-phase rectifier systems is therefore discussed and analysed.

A. Averaged Output Voltage V_o

In general, time instants where a passive three-phase rectifier is initiating the commutation process between two different phases is defined by $\frac{2\cdot(k-1)\pi}{3}$ ($k \in \mathbb{Z}$), if well-balanced mains voltages are assumed. Due to the fact, that these time instants are dependent on the mains voltage situation they may easily compute to

$$\begin{aligned} x_{t12,k} &= \pi \cdot k + \arctan\left(\frac{1}{\sqrt{3}}\,\frac{2\hat{V}_{N1}+\hat{V}_{N2}}{\hat{V}_{N2}}\right) \\ x_{t23,k} &= \pi \cdot k + \arctan\left(\frac{1}{\sqrt{3}}\,\frac{\hat{V}_{N2}-\hat{V}_{N3}}{\hat{V}_{N2}+\hat{V}_{N3}}\right) \\ x_{t31,k} &= \pi \cdot k - \arctan\left(\frac{1}{\sqrt{3}}\,\frac{2\hat{V}_{N1}+\hat{V}_{N3}}{\hat{V}_{N3}}\right) \end{aligned} \tag{22}$$

with $k \in \mathbb{Z}$ if imbalance in grid voltages is expected. x_{tij} denotes the respective time instant where $v_{Ni}(\varphi_N) = v_{Nj}(\varphi_N)$ for $i \neq j$.[2] **Fig. 3** depicts the discussed unsymmetrical mains situation and shows the computed commutation time instants, which are slightly differing from the typical well-known 60° transitions. It has to be noted that the given equations are furthermore valid for perfectly aligned mains $V_{N1,rms} = V_{N2,rms} = V_{N3,rms} = V_{N,rms}$ which can be demonstrated by

$$\begin{aligned} x_{t12,0} &= \pi \cdot 0 + \arctan\left(\frac{1}{\sqrt{3}}\,\frac{2\hat{V}_{N1}+\hat{V}_{N2}}{\hat{V}_{N2}}\right) \\ &= \arctan\left(\sqrt{3}\right) = \frac{\pi}{3}. \end{aligned} \tag{23}$$

Calculated time instants ($x_{t31,0}$, $x_{t12,0}\dots$) can now be used to analytially evaluate the emerging DC-output voltage V_o for unbalanced mains voltages.

$$\begin{aligned} V_o = \frac{1}{\pi}\Bigg(&\int_{x_{t31,0}}^{x_{t12,0}} v_{N1}(\varphi_N)\,\mathrm{d}\varphi_N + \int_{x_{t12,0}}^{x_{t23,1}} v_{N2}(\varphi_N)\,\mathrm{d}\varphi_N + \dots \\ &\dots + \int_{x_{t23,1}}^{x_{t31,2}} v_{N3}(\varphi_N)\,\mathrm{d}\varphi_N \Bigg) \end{aligned} \tag{24}$$

Considering a number of addition theorems as

- $\sin(-\varphi_N) = -\sin(\varphi_N)$
- $\sin(\arctan(\varphi_N)) = \frac{\varphi_N}{\sqrt{1+\varphi_N^2}}$
- $\cos(\arctan(\varphi_N)) = \frac{1}{\sqrt{1+\varphi_N^2}}$
- $\sin(\varphi_x - \varphi_y) = \sin(\varphi_x)\cos(\varphi_y) - \cos(\varphi_x)\sin(\varphi_y)$

the averaged output voltage V_o yields

$$\begin{aligned} V_o = \frac{1}{\pi}\Big(&\sqrt{\hat{V}_{N1}^2 + \hat{V}_{N1}\hat{V}_{N2} + \hat{V}_{N2}^2} + \dots \\ &\dots + \sqrt{\hat{V}_{N1}^2 + \hat{V}_{N1}\hat{V}_{N3} + \hat{V}_{N3}^2} + \dots \\ &\dots + \sqrt{\hat{V}_{N2}^2 + \hat{V}_{N2}\hat{V}_{N3} + \hat{V}_{N3}^2}\Big). \end{aligned} \tag{25}$$

Expecting a supply voltage imbalance of 2 %, the averaged output voltage varies by approximately 0.4 % (< 2 V). In order to demonstrate general validity of (25), balanced mains voltages are assumed ($V_{N1,rms} = V_{N2,rms} = V_{N3,rms} = V_{N,rms}$) and result in the widely known

$$\begin{aligned} V_{o,unbal} = \frac{1}{\pi}\Big(&\sqrt{\hat{V}_N^2 + \hat{V}_N\hat{V}_N + \hat{V}_N^2} + \dots \\ &\dots + \sqrt{\hat{V}_N^2 + \hat{V}_N\hat{V}_N + \hat{V}_N^2} + \dots \\ &\dots + \sqrt{\hat{V}_N^2 + \hat{V}_N\hat{V}_N + \hat{V}_N^2}\Big) = \frac{3\sqrt{3}\hat{V}_N}{\pi}. \end{aligned} \tag{26}$$

B. DC-Side Inductance Current

The analytical gained knowledge acquired due to mathematical investigations of V_o for unbalanced mains voltage conditions can be exploited to evaluate the "sector by sector" characteristics of the DC-side smoothing inductance current (i_L). It must be noted that the calculated inductor current shows $\frac{\pi}{3}$-periodic current characteristics for balanced input voltage waveforms. The DC-side smoothing choke current for unbalanced mains voltage conditions, obviously results in π-periodicity (cf., **Fig. 4**). The

[2] $i = 1, 2, 3$, $j = 1, 2, 3$. Both indices i and j indicate one of the three mains phase numbers.

inductor current ($i_{\mathrm{L,unbal}}$) is given by

$$\begin{aligned} i_{\mathrm{L,unbal}}\left(\varphi_{\mathrm{N}}\right) = I_{\mathrm{o,unbal}} - \frac{V_{\mathrm{o}}}{\omega_{\mathrm{N}} L_{\mathrm{DC}}}\left(\varphi_{\mathrm{N}} - x_{\mathrm{t23,0}}\right) + \ldots \\ \ldots + \frac{2\hat{V}_{\mathrm{N1}} + \hat{V}_{\mathrm{N3}}}{2\omega_{\mathrm{N}} L_{\mathrm{DC}}}\left(\sin\left(\varphi_{\mathrm{N}}\right) - \sin\left(x_{\mathrm{t23,0}}\right)\right) - \ldots \\ \ldots - \frac{\sqrt{3}\hat{V}_{\mathrm{N3}}}{2\omega_{\mathrm{N}} L_{\mathrm{DC}}}\left(\cos\left(\varphi_{\mathrm{N}}\right) - \cos\left(x_{\mathrm{t23,0}}\right)\right) \end{aligned} \tag{27}$$

for 10 kW output power, a sector of $\varphi_{\mathrm{N}} \in [x_{\mathrm{t23,0}} \ldots x_{\mathrm{t12,0}}]$ and an averaged output voltage $V_{\mathrm{o,unbal}}$ as derived in (25). $I_{\mathrm{o,unbal}}$ denotes the adapted constant output current

$$I_{\mathrm{o,unbal}} = \frac{P_{\mathrm{o}}}{V_{\mathrm{o,unbal}}}\,. \tag{28}$$

For the given equation the output load has been considered to be highly inductive ($I_{\mathrm{o}} \approx \mathrm{const}$) and the output capacitor $C_{\mathrm{o}} \to \infty$. The output voltage ripple is hence assumed to be 0 V. Finally, it has to be demonstrated that the means of the computed current waveforms still equal the calculated output current $I_{\mathrm{o,unbal}}$:

$$\begin{aligned} I_{\mathrm{L,unbal,avg}} = \frac{1}{\pi}\Bigg(\int_{x_{\mathrm{t31,0}}}^{x_{\mathrm{t12,0}}} i_{\mathrm{L,unbal}}\left(\varphi_{\mathrm{N}}\right)\,\mathrm{d}\varphi_{\mathrm{N}} + \ldots \\ \ldots + \int_{x_{\mathrm{t12,0}}}^{x_{\mathrm{t23,1}}} i_{\mathrm{L,unbal}}\left(\varphi_{\mathrm{N}}\right)\,\mathrm{d}\varphi_{\mathrm{N}} + \ldots \\ \ldots + \int_{x_{\mathrm{t23,1}}}^{x_{\mathrm{t31,2}}} i_{\mathrm{L,unbal}}\left(\varphi_{\mathrm{N}}\right)\,\mathrm{d}\varphi_{\mathrm{N}} \Bigg) \\ = \frac{P_{\mathrm{o}}}{V_{\mathrm{o,unbal}}} = I_{\mathrm{o,unbal}} \end{aligned} \tag{29}$$

Fig. 4 illustrates the DC-side inductance currents of a hybrid rectifier system employing third harmonic injection for unbalanced mains voltages and a nominal output power of 10 kW. Three different mains voltage conditions are considered:

- the perfectly balanced voltage situation,
- a devation of mains peak voltages of $\pm 1\%$
- and a devation of mains peak voltages of $\pm 3\%$.

As can be seen in **Fig. 4**, the peak-to-peak current ripple of i_{L} is tremendously increasing, even for small mains voltage imbalance errors. Considering symmetric mains voltages a peak-to-peak current ripple of

$$\Delta I_{\mathrm{L,pkpk}} = 14.4\,\mathrm{A} \tag{30}$$

appears for $P_{\mathrm{o}} = 10\,\mathrm{kW}$, $L_{\mathrm{DC}} = 2.25\,\mathrm{mH}$, $V_{\mathrm{N,rms}} = 230\,\mathrm{V}$. If unbalanced mains conditions are, however, expected ($V_{\mathrm{N,rms}} \pm 1\%$ and $V_{\mathrm{N,rms}} \pm 3\%$) the 300 Hz DC-side choke peak-to-peak current ripple computes to

$$\Delta I_{\mathrm{L,pkpk,unbal}\pm 1\%} = 18.2\,\mathrm{A} \tag{31}$$

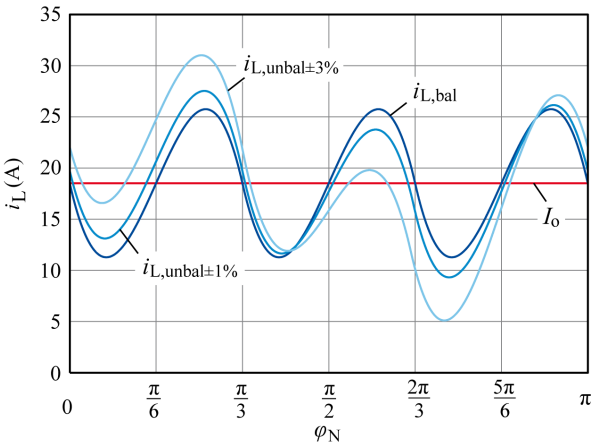

Fig. 4: DC-side smoothing inductor current i_{L} for balanced mains and grid voltage deviations of $\pm 1\%$ and $\pm 3\%$ ($i_{\mathrm{L,bal}}$, $i_{\mathrm{L,unbal}\pm 1\%}$ and $i_{\mathrm{L,unbal}\pm 3\%}$, respectively) considering a DC-side smoothing inductance L_{DC} of 2.25 mH, an output power of 10 kW and a constant output voltage V_{o}.

and

$$\Delta I_{\mathrm{L,pkpk,unbal}\pm 3\%} = 26.4\,\mathrm{A}, \tag{32}$$

respectively. For a grid voltage deviation of $\pm 1\%$ and $\pm 3\%$ i_{L} shows an augmented peak-to-peak current ripple of 26% and 83%, respectively. It has to be noted that these results are assuming an infinitely high output capacitor ($C_{\mathrm{out}} \to \infty$) which results in a purely DC voltage component of v_{o} ($= V_{\mathrm{o}}$). If real capacitor values of C_{o} are supposed, the emerging low harmonic output voltage ripple is inconveniently affecting the DC-side inductor current ripple. $I_{\mathrm{L,pkpk}}$ can, therefore, be presumed to be even higher than the previously computed results.
To put it in a nutshell, unbalanced mains voltages lead to a superimposed 100 Hz voltage component in the DC-side output filter of the passive rectifier circuit which results in increased peak-to-peak current ripple of the DC-side smoothing inductance current i_{L} and consequently augmented low harmonic AC voltage components of the rectifiers output capacitor (C_{o}).

C. Effects on Active Current Injection Cell

The optionally active rectifier – which allows the extension of a passive rectifier to a low harmonic input stage – is basically injecting some amount of current into the positive and negative busbar of the passive rectifier which guarantees sinusoidal waveshapes i_{pos} and i_{neg} (cf., **Fig. 1**). The 300 Hz (and evoked 100 Hz) current component of i_{L} has hence to be compensated by the equipped injection circuit. A simulation model has therefore been implemented (cf., **Fig. 5(a)**) in order to demonstrate the effects of imbalance in grid voltages on the equipped active enhancement. Considered main passive components for the 10 kW/10 kHz simulation model are as follows:

- Current Injection Circuit - FCC
- $L_{\mathrm{c}} = 1.8\,\mathrm{mH}$
- $C_{\mathrm{f}} = 6.8\,\mu\mathrm{F}$
- $L_{\mathrm{DC}} = 2.25\,\mathrm{mH}$
- $C_{\mathrm{o,p}} = C_{\mathrm{o,n}} = 2.2\,\mathrm{mF}$
- $R_{\mathrm{sym}} = 47\,\mathrm{k\Omega}$.

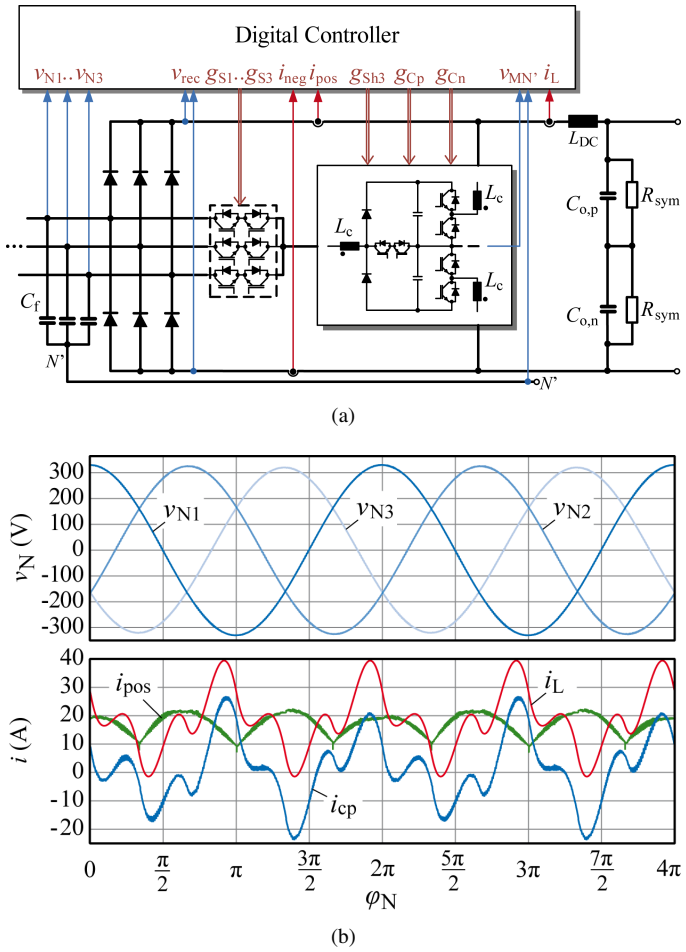

Fig. 5: (a) Implemented simulation model of hybrid rectifier topology in order to discuss effects of unbalanced mains voltages on current injection devices employing third harmonic injection principle. (b) Simulation results of a 10 kW/10 kHz hybrid rectifier utilizing a FCC. Unbalance of mains voltages is defined by $V_{N,rms} \pm 3\%$. Output capacitor is defined by $C_{o,p} = C_{o,n} = 2.2\,\mathrm{mF}$.

Current and voltage controllers of converter topologies are implemented as described in [20] and [22]. Imbalance in mains voltages is defined by $V_{N,rms} \pm 3\%$. **Fig. 5(b)** depicts simulation results of injection current i_{cp}, DC-side smoothing inductance current i_L and positive busbar current i_{pos}. As can be seen, i_L shows the previously discussed increased peak-to-peak current ripple which is approximately 41 A for the given configuration. For both, the balanced and slightly unbalanced grid voltage condition, sinusoidal input peak currents ($\hat{I}_N$) are supposed to be $\approx$ 20 A for 10 kW output power considering proper current control of the rectifier. For the well-balanced condition this results in an injection current i_{cp} with the following characteristics:

- peak current $\hat{I}_{cp} \approx 12\,\mathrm{A}$
- peak-to-peak current $\Delta I_{cp} \approx 20\,\mathrm{A}$
- rms current $I_{cp,rms} \approx 6\,\mathrm{A}$
- averaged current $I_{cp,avg} \approx 1.6\,\mathrm{A}$.

An input voltage unbalance of $V_{N,rms} \pm 3\%$ is, however, causing tremendously impaired injection current i_{cp} (and i_{cn}) characteristics which are now defined by

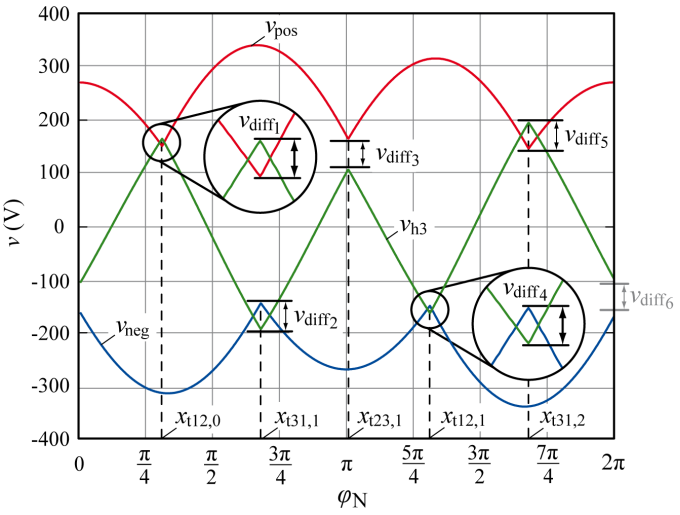

Fig. 6: Calculated waveforms of positive and negative output voltage v_{pos} and v_{neg} of the hybrid rectifier and third harmonic voltage v_{h3}. $x_{tij,k}$ denotes adapted commutation time instants for unbalanced mains voltage condition. v_{diff} indicates multiple transition mismatches due to unbalanced mains voltages.

- peak current $\hat{I}_{cp} \approx 26\,\mathrm{A}$ (+116%)
- peak-to-peak current $\Delta I_{cp} \approx 50\,\mathrm{A}$ (+150%)
- rms current $I_{cp,rms} \approx 12\,\mathrm{A}$ (+100%)
- averaged current $I_{cp,avg} \approx 1.6\,\mathrm{A}$. ($\approx$ +0%)

The modified current characteristics, furthermore, result in diminished overall efficiency η_{sys} of the total system due to increased switching and conduction losses of active components and additional resistive losses of passive components. Moreover, increased iron losses of DC-side smoothing and injection inductors can be expected.

IV. Effects of Heavily Unbalanced Mains Voltages on THD of Input Currents

As already noted, unbalanced mains voltages can highly affect DC-side current and voltage waveforms and may even inflict design considerations of the hybrid system. Depending on the implemented control method of the rectifier, imbalance in grid voltages can furthermore worsen total harmonic distortions (THD) of input currents ($i_{N,i}$). In order to highlight the impact on input currents, heavily unbalanced mains ($\pm 20\,\%$) voltages are assumed for illustration.

Using adapted commutation time instants for unbalanced mains voltage conditions $x_{tij,k}$ (according to (22)), positive and negative output voltage waveforms v_{pos} and v_{neg} can be easily determined and are illustrated in **Fig. 6**. The third harmonic voltage v_{h3} is defined by the rectifiers output voltage situation of v_{pos} and v_{neg} and hence given by

$$v_{h3} = -v_{pos} - v_{neg}\,. \tag{33}$$

As shown in **Fig. 6**, signal waveforms of v_{h3} and v_{pos} (and v_{h3} and v_{neg}) are not matching anymore for those time instants where the voltage transition of two different phases of the passive diode bridge appears. This observed deflection is defined as v_{diff} (cf., **Fig. 6**) and occurs at the respective current commutation time instant $x_{tij,k}$. The first voltage mismatch

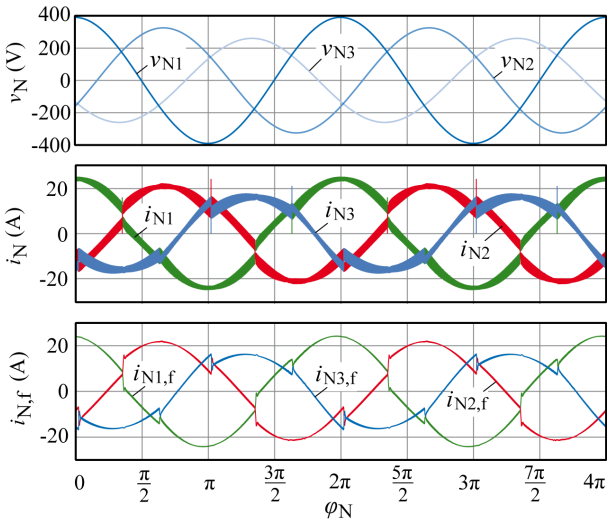

Fig. 7: Simulation results of a 10 kW/10 kHz hybrid rectifier utilizing a FCC for heavily unbalanced mains voltages ($V_{N,rms} \pm 20\%$). Filtered AC input currents $i_{Ni,f}$ result in $THD_{i,1} = 10.2\,\%$, $THD_{i,2} = 15.5\,\%$ and $THD_{i,1} = 12.86\,\%$

$v_{diff,1}$ can be assessed by

$$v_{diff,1} = v_{pos}\left(x_{t12,0}\right) - v_{h3}\left(x_{t12,0}\right) \tag{34}$$

with $v_{h3}\left(x_{t12,0}\right) = -v_{pos}\left(x_{t12,0}\right) - v_{neg}\left(x_{t12,0}\right)$. $v_{diff,1}$ can therefore be computed to

$$v_{diff,1} = \frac{\sqrt{3}}{2} \frac{2\hat{V}_{N1}\hat{V}_{N2} - \hat{V}_{N1}\hat{V}_{N3} - \hat{V}_{N2}\hat{V}_{N3}}{\sqrt{\hat{V}_{N1}^2 + \hat{V}_{N1}\hat{V}_{N2} + \hat{V}_{N2}^2}} \,. \tag{35}$$

All remaining voltage deviations $v_{diff,2} - v_{diff,6}$ can be calculated similarly under consideration of (34). It has to be noted that $v_{diff,1} = v_{diff,4}$, $v_{diff,2} = v_{diff,5}$ and $v_{diff,3} = v_{diff,6}$.
These voltage deviations are of major importance for generation of current and voltage controller reference signals of the active current injection cell. In conventional active rectifier circuits [18], the reference currents are often generated by a superimposed voltage controller which indirectly determines the power demand by measuring the voltage of the dc-link capacitor. The output voltage of the proposed rectifier system is, however, not controlled, but is dependent on the mains and load situation and is even not measured. The power transferred from the mains to the output of the rectifier is not dependent on the current shape and can therefore be determined by measurement in both operating modes, operating in diode mode as well as for active current shaping using the FCC. The power demand can be determined using the mains voltages (v_{N1}, v_{N2}, v_{N3}) and DC-side current i_L

$$p(t) = \left(v_{pos} - v_{neg}\right) i_L \,. \tag{36}$$

The equivalent conductance g_e^* can now be calculated to

$$g_e^* = \frac{P_{in}}{V_{N1,rms}^2 + V_{N2,rms}^2 + V_{N3,rms}^2} \,. \tag{37}$$

P_{in} is the low-pass filtered constant value of instantaneous power demand $p(t)$. g_e^* is finally multiplied with the (calculated) voltages v_{pos} and v_{neg} in order to derive the reference currents i_{pos}^* $(= g_e^* v_{pos})$ and i_{neg}^*. As

$$i_{pos} + i_{h3} + i_{neg} = 0 \tag{38}$$

the same mismatch applicable for DC-side voltages v_{pos}, v_{h3} and v_{neg} is also valid for DC-side currents i_{pos}, i_{h3} and i_{neg}. The input currents are therefore supposed to show current steps during every current transition of the input side of the system. Simulation results of the discussed issues are illustrated in **Fig. 7** for heavily unbalanced mains voltages of $V_{N1,rms} = 276\,V$, $V_{N2,rms} = 230\,V$ and $V_{N3,rms} = 184\,V$. Filtered AC input currents $i_{Ni,f}$ finally result in a total harmonic distortion of $THD_{i,1} = 10.2\,\%$, $THD_{i,2} = 15.5\,\%$ and $THD_{i,1} = 12.86\,\%$ which is significantly higher than the officially allowed 5 % according to IEEE standards.

TABLE II: Power Devices Selected for Implementation of the FCC Prototype.

$S_{ia,b}$	1200 V/40 A IGBT, IKW40T120, Infineon
$S_{c\frac{p}{n}\pm}$	600 V/20 A IGBT, IKW20N60H3, Infineon
$D_{h3\pm}$	1200 V/15 A, STTH1512W, ST-Microelectronics
$C_{c\frac{p}{n}}$	470 μF/400 V, EPCOS B43501-type
L_{cp}=L_{cn}=L_{h3}	3.2 mH, Iron core 3UI60a, N = 123 turns
C_F, C_S	6.8 μF/275 V_{AC}, MKP X2, Arcotronics
C_o	2.2 mF/400 V, Felsic CO 39 A728848
L_{DC}	2.25 mH, Iron core 2 x UI60a
$D_1 - D_6$	35 A/1600 V, 36MT160, Vishay

V. Experimental Results

Measurement results of the constructed 10 kW/10 kHz laboratory prototype for 50 Hz/400 V_{LL} mains are illustrated in **Fig. 8**. The applied components of the hybrid system are listed in TABLE II. Measurement taken from a three-phase grid at the power electronics laboratory of the Vienna university of technology revealed a THD_v of approximately 2 % and an maximum grid unbalance of less than 1 %. A detailed characterisation of fundamental components and higher harmonics of all three mains phases are listed TABLE III. All results have been obtained by a PM-300 power analyser.
Fig. 8 clearly reveals the discussed superimposed 100 Hz component of i_L which obviously results in an increased peak-to-peak current ripple $\Delta I_{L,pkpk} = 21\,A$. This furthermore leads to an increased injection current i_{cp} showing a peak-to-peak current ripple $\Delta I_{cp,pkpk}$ of 28 A instead of the expected 21 A.

VI. Conclusion

Effects of unbalanced AC-side mains voltages on passive three-phase rectifier systems, which are utilizing a current injection device (in order to guarantee sinusoidal input currents), have been analysed in this paper. It is shown that even slightly imbalanced mains voltages may result in significantly increased DC-side smoothing inductance (L_{DC}) current ripple and hence injection inductance (L_c) current ripple. Reduced efficiency and even overload condition of the system can therefore be expected due to higher switching and conduction losses of active components, as well as additional resistive losses of passive components and iron losses of inductors.

TABLE III: Measured Mains Voltage Harmonics (Location: Vienna University of Technology - Power Electronics Laboratory).

Measured Harmonic Components of Mains Voltages			
	v_{N1}	v_{N2}	v_{N3}
Fund. Comp.	231.3 V	230.5 V	229.9 V
3^{rd} ord. harm.	0.33%	0.09%	0.41%
5^{th} ord. harm.	2.22%	2.19%	2.06%
7^{th} ord. harm.	1.32%	1.22%	1.29%
9^{th} ord. harm.	0.22%	0.37%	0.43%
11^{th} ord. harm.	0.22%	0.41%	0.33%
13^{th} ord. harm.	0.47%	0.56%	0.53%
15^{th} ord. harm.	0.14%	0.21%	0.31%
17^{th} ord. harm.	0.16%	0.23%	0.19%

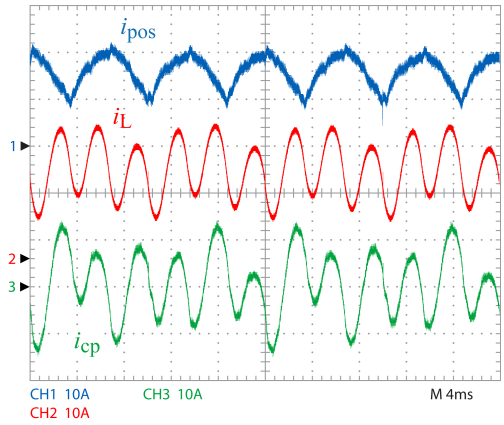

Fig. 8: Measured currents i_{pos}, i_L and i_{cp} for an output power of $P_o = 10\,kW$ and fundamental mains voltage components of $V_{N1,rms} = 231.3\,V$, $V_{N2,rms} = 230.5\,V$ and $V_{N3,rms} = 229.9\,V$.

The output voltage of the system (v_o) is characterized by a superimposed 100 Hz voltage spectral component in addition to its preliminary dominant DC and 300 Hz voltage components. It is furthermore shown, that imbalance in mains voltages impairs input currents total harmonic distortion characteristics. An appropriate control strategy for hybrid rectifiers employing third harmonic injection considering heavily unbalanced mains voltage condition is not discussed up to now and should hence be topic of further research.

REFERENCES

[1] N. Mohan, "A Novel Approach to Minimize Line-Current Harmonics in Interfacing Power Electronics Equipment with 3-Phase Utility Systems," *IEEE Transactions on Power Delivery*, vol. 8, no. 3, pp. 1395–1401, 1993.

[2] P. Pejovic and Z. Janda, "Optimal Current Programming in Three-Phase High-Power-Factor Rectifier Based on Two Boost Converters," *IEEE Transactions on Power Electronics*, vol. 13, no. 6, pp. 1152–1163, 1998.

[3] T.B. Soeiro, T. Friedli, and J.W. Kolar, "Swiss Rectifier — A Novel Three-Phase Buck-Type PFC Topology for Electric Vehicle Battery Charging," in *Proceedings of the Twenty-Seventh Annual IEEE Applied Power Electronics Conference and Exposition (APEC)*, 2012, pp. 2617–2624.

[4] J.W. Kolar, H. Ertl, and Franz C. Zach, "A novel three-phase single-switch discontinuous-mode AC-DC buck-boost converter with high-quality input current waveforms and isolated output," vol. 9, no. 2, pp. 160–172, 1994.

[5] F. Stogerer, J. Minibock, and J.W. Kolar, "Implementation of a Novel Control Concept for Reliable Operation of a VIENNA Rectifier under Heavily Unbalanced Mains Voltage Conditions," in *Proceedings of the IEEE 32nd Annual Power Electronics Specialists Conference (PESC)*, 2001, vol. 3, pp. 1333–1338.

[6] J. Minibock, R. Greul, and J.W. Kolar, "A Novel Control Concept for Operating a Two-Stage Delta-Rectifier-Based Telecommunications Power Supply Module under Heavily Unbalanced Mains Voltage Conditions," in *Proceedings of the Seventeenth Annual IEEE Applied Power Electronics Conference and Exposition (APEC)*, 2002, vol. 2, pp. 716–721.

[7] M. Baumann and J.W. Kolar, "A Novel Control Concept for Reliable Operation of a Three-Phase Three-Switch Buck-Type Unity-Power-Factor Rectifier with Integrated Boost Output Stage under Heavily Unbalanced Mains Condition," *IEEE Transactions on Industrial Electronics*, vol. 52, no. 2, pp. 399–409, 2005.

[8] H.M. Teshnizi, A. Moallem, M.-R. Zolghadri, and M. Ferdowsi, "A Dual-Frame Hybrid Vector Control of Vector Modulated VIENNA I Rectifier for Unity Power Factor Operation under Unbalanced Mains Condition," in *Proceedings of Twenty-Third Annual IEEE Applied Power Electronics Conference and Exposition (APEC)*, 2008, pp. 1402–1408.

[9] Lei Shang, Dan Sun, Jiabing Hu, and Yikang He, "Predictive Direct Power Control of Grid-Connected Voltage-Sourced Converters under Unbalanced Grid Voltage Conditions," in *Proceedings of the International Conference on Electrical Machines and Systems (ICEMS)*, 2009, pp. 1–5.

[10] Zheng Zheng and Zhang Zhen-hua, "Research of Direct Power Control for PWM Rectifier under Unbalanced Grid Voltage," in *Proceedings of the 25th Chinese Control and Decision Conference (CCDC)*, 2013, pp. 3607–3612.

[11] Y. Zhang, C. Qu, Z. Li, and Yingchao Zhang, "Direct Power Control of PWM Rectifier under Unbalanced Grid Voltage," in *Proceedings of the 17th International Conference on Electrical Machines and Systems (ICEMS)*, 2014, pp. 3199–3204.

[12] Y. Zhang and C. Qu, "Direct Power Control of a Pulse Width Modulation Rectifier Using Space Vector Modulation Under Unbalanced Grid Voltage," *IEEE Transactions on Power Electronics*, 2014, Early Access.

[13] Y. Zhang and C. Qu, "Table-Based Direct Power Control for Three-Phase AC/DC Converters Under Unbalanced Grid Voltages," *IEEE Transactions on Power Electronics*, 2015, Early Access.

[14] Y. Zhang and C. Qu, "Model Predictive Direct Power Control of PWM Rectifier Under Unbalanced Network Conditions," *IEEE Transactions on Industrial Electronics*, 2015, Early Access.

[15] H. Abaali, M.T. Lamchich, and M. Raoufi, "The Three Phase Shunt Active Filters for the Harmonics Compensation under Distorted and Unbalanced Mains Voltages Conditions," in *Proceedings of the IEEE International Conference onIndustrial Technology (ICIT)*, 2004, vol. 1, pp. 558–563.

[16] D. De and V. Ramanarayanan, "An Active Shunt Compensator for Reactive, Unbalanced and Harmonic Loads under Balanced and Unbalanced Grid Voltage Conditions," in *Proceedings of the International Conference on Power Electronics, Drives and Energy Systems (PEDES)*, 2010, pp. 1–6.

[17] X. Liu, F. Blaabjerg, P.C. Loh, and P. Wang, "Carrier-Based Modulation Strategy and Its Implementation for Indirect Matrix Converter under Unbalanced Grid Voltage Conditions," in *Proceedings of the 15th International Power Electronics and Motion Control Conference (EPE/PEMC)*, 2012.

[18] J.W. Kolar and T. Friedli, "The Essence of Three-Phase PFC Rectifier Systems—Part I," *IEEE Transactions on Power Electronics*, vol. 28, no. 1, pp. 176–198, 2013.

[19] M. Hartmann and R. Fehringer, "Active Three-Phase Rectifier System Using a "Flying" Converter Cell," in *Proceedings of the International Energy Conference and Exhibition (ENERGYCON)*, 2012, pp. 82–89.

[20] M. Hartmann, R. Fehringer, M. Makoschitz, and H. Ertl, "Design and Experimental Verification of a Third Harmonic Injection Rectifier Circuit Using a Flying Converter Cell," in *Proceedings of the Twenty-Ninth Annual IEEE Applied Power Electronics Conference and Exposition (APEC)*, 2014, pp. 920–927.

[21] M. Makoschitz, M. Hartmann, and H. Ertl, "Analysis of a Three-Phase Flying Converter Cell Rectifier Operating in Light/No-Load Condition," in *Proceedings of the 30th Annual IEEE Applied Power Electronics Conference and Exposition (APEC)*, 2015, pp. 920–927.

[22] M. Makoschitz, M. Hartmann, H. Ertl, and R. Fehringer, "DC Voltage Balancing of Flying Converter Cell," in *Proceedings of the Energy Conversion Congress and Exposition (ECCE)*, 2014, pp. 4071–4078.